Antiferroelectric properties and site occupations of cations in luminescent host materials

Accepted Manuscript

Antiferroelectric properties and site occupations of R^{3+} cations in $Ca_8MgR(PO_4)_7$ luminescent host materials

Alexei A. Belik, Vladimir A. Morozov, Dina V. Deyneko, Alexander E. Savon, Oksana V. Baryshnikova, Evgeniya S. Zhukovskaya, Nikolay G. Dorbakov, Yoshio Katsuya, Masahiko Tanaka, Sergey Yu Stefanovich, Joke Hadermann, Bogdan I. Lazoryak

PII: S0925-8388(16)34217-7

DOI: 10.1016/j.jallcom.2016.12.288

Reference: JALCOM 40210

To appear in: *Journal of Alloys and Compounds*

Received Date: 26 September 2016

Revised Date: 21 December 2016

Accepted Date: 22 December 2016

Please cite this article as: A.A. Belik, V.A. Morozov, D.V. Deyneko, A.E. Savon, O.V. Baryshnikova, E.S. Zhukovskaya, N.G. Dorbakov, Y. Katsuya, M. Tanaka, S.Y. Stefanovich, J. Hadermann, B.I. Lazoryak, Antiferroelectric properties and site occupations of R^{3+} cations in $Ca_8MgR(PO_4)_7$ luminescent host materials, *Journal of Alloys and Compounds* (2017), doi: 10.1016/j.jallcom.2016.12.288.

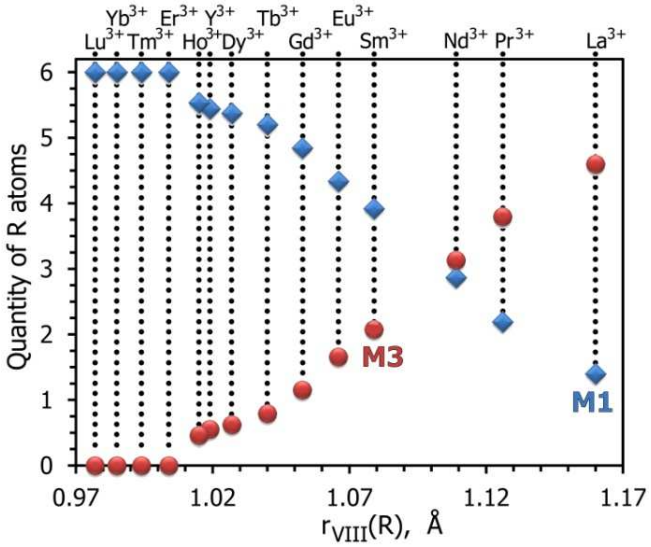

Antiferroelectric properties and site occupations of R^{3+} cations in $Ca_8MgR(PO_4)_7$ luminescent host materials

Alexei A. Belik[a,*], Vladimir A. Morozov[b,c], Dina V. Deyneko[b,d], Alexander E. Savon[e], Oksana V. Baryshnikova[b], Evgeniya S. Zhukovskaya[b], Nikolay G. Dorbakov[b], Yoshio Katsuya[f], Masahiko Tanaka[f], Sergey Yu. Stefanovich[b], Joke Hadermann[c], Bogdan I. Lazoryak[b]

[a]*Research Center for Functional Materials, National Institute for Materials Science, Namiki 1-1, Tsukuba, Ibaraki 305-0044, Japan*

[b]*Chemistry Department, Moscow State University, 119991 Moscow, Russia*

[c]*EMAT, University of Antwerp, Groenenborgerlaan 171, B-2020, Belgium*

[d]*Shubnikov Institute of Crystallography RAS, 119333 Moscow, Russia*

[e]*Skobeltsyn Institute of Nuclear Physics, Moscow State University, 119991 Moscow, Russia*

[f]*Synchrotron X-ray Station at SPring-8, NIMS, Kouto 1-1-1, Sayo-cho, Hyogo 679-5148, Japan.*

* Corresponding author Alexei.BELIK@nims.go.jp

Abstract

$Ca_8MgR(PO_4)_7$ (R = La, Pr, Nd, Sm–Lu, and Y) phosphates with a β-$Ca_3(PO_4)_2$ related structure were prepared by a standard solid-state method in air. Second-harmonic generation, differential scanning calorimetry, and dielectric measurements led to the conclusion that all $Ca_8MgR(PO_4)_7$ are centrosymmetric and go to another centrosymmetric phase in the course of a first-order antiferroelectric phase transition well above room temperature (RT). High-temperature electron diffraction showed that the symmetry changes from $R\bar{3}c$ to $R\bar{3}m$ during the phase transition. Structures of $Ca_8MgR(PO_4)_7$ at RT were refined by the Rietveld method in centrosymmetric space group $R\bar{3}c$. Mg^{2+} cations occupy the $M5$ site; the occupancy of the $M1$ site by R^{3+} cations increases monotonically from 0.0389 for R = La to 0.1667 for R = Er-Lu, whereas the occupancy of the $M3$ site by R^{3+} cations decreases monotonically from 0.1278 for R = La to 0 for R = Er-Lu. In the case of R = Er-Lu, the $M3$ site is occupied only by Ca^{2+} cations. $P1O_4$ tetrahedra and cations at the $M3$ site are disordered in the $R\bar{3}c$ structure of $Ca_8MgR(PO_4)_7$. Using synchrotron X-ray powder diffraction, we found that annealing conditions do not significantly affect the distribution of Ca^{2+} and Eu^{3+} cations between the structure positions of $Ca_8MgEu(PO_4)_7$. Luminescent properties of $Ca_8MgEu(PO_4)_7$ powder samples were investigated under near-ultraviolet (n-UV) light. Excitation spectra of $Ca_8MgEu(PO_4)_7$ show the strongest absorption at about 395 nm that matches with commercially available n-UV-emitting GaN-based LED chips. Emission spectra show an intense red emission due to the $^5D_0 \rightarrow {}^7F_2$ transition of Eu^{3+}.

Keywords: Optical materials; Inorganic materials; Solid state reactions; Crystal structure; Luminescence; Synchrotron radiation.

1. Introduction

Multifunctional materials can be defined as those possessing specific desirable electronic, magnetic, optical, thermal, or other properties in one material. β-$Ca_3(PO_4)_2$-related compounds [1], e.g., $Ca_9R(AO_4)_7$ and $Ca_8MgR(AO_4)_7$ (*A* = P and V; *R* = Sc, Cr, Ga, In, Y, and rare-earth (RE) cations), are examples of such multifunctional materials. They were found to be promising as light-emitting diodes (LED) [2, 3], laser [4], and non-linear optical materials [5-7]. Moreover, these compounds are known as ferroelectrics [5-7] and antiferroelectrics [8, 9], catalysts [10], and biomaterials [11].

The β-$Ca_3(PO_4)_2$-type structure (space group (SG): *R*3*c*, *Z* = 21) consists of isolated PO_4 tetrahedra that connect CaO_n polyhedra into a 3D framework via common vertices [1]. Ca^{2+} cations occupy five positions: *M*1–*M*5; the *M*1–*M*3 (18-fold) and *M*5 (6-fold) positions are fully occupied whereas *M*4 (6-fold) and *M*6 (6-fold) sites are half-occupied and vacant, respectively. The peculiarity of the structure is the ability to accommodate different cations with size and charge variations without significant changes of the framework. Size variations of the CaO_n polyhedra in the β-$Ca_3(PO_4)_2$ structure allow a large variety of isovalent and aliovalent substitutions for Ca^{2+} cations [12-19]. Depending on the ionic radius, replacing cations substitute Ca^{2+} in different positions. Small size cations, such as Mg^{2+}, Fe^{3+}, Ni^{2+} and Cu^{2+}, substitute Ca^{2+} in the *M*4 and *M*5 sites [8, 14, 15, 19] whereas large size cations, such as RE cations, replace Ca^{2+} in the *M*1–*M*3 or *M*1, *M*2, and *M*5 sites [12]. Monotonic changes of the *M*1–*M*3 and *M*5 site occupancies by R^{3+} cations have been found in $Ca_9R(AO_4)_7$ compounds with *A* = V [12, 20-22] and P [23]. An overview of cation distributions among the *M*1–*M*5 sites of the β-$Ca_3(PO_4)_2$ structure is given in Ref. [24].

Phosphors for LEDs should preferably be a single-phase material and contain different RE or other luminescent cations. $Ca_8MgR(PO_4)_7$ compounds have the structure-forming RE cations, and they can be additionally doped by a large variety of luminescent cations. For this reason, $Ca_8MgR(PO_4)_7$ (*R* = RE and Y) compounds have been intensively studied recently as potential luminescence materials [25-32]. Recent examples include compounds doped or co-doped with Eu^{3+} [25, 26, 33-35], Eu^{2+} [27, 36, 37], Tb^{3+} [38], Dy^{3+} [3, 31, 39], Pr^{3+} [40], Sm^{3+} [41], Tb^{3+}/Eu^{3+} [42], Tb^{3+}/Mn^{2+} [28], Ce^{3+}/Mn^{2+} [29], Eu^{2+}/Mn^{2+} [30, 43-45], $Ce^{3+}/Tb^{3+}/Mn^{2+}$ [32], $Ce^{3+}/Eu^{2+}/Mn^{2+}$ [46], and $Yb^{3+}/Er^{3+}/Ho^{3+}/Tm^{3+}$ [44]. The introduction of one or several doped cations preserves the structure and creates multi-colored and tunable phosphors. To give a correct description of luminescent properties it is necessary to know the structure of $Ca_8MgR(PO_4)_7$ compounds and to have information about polyhedra occupied by RE cations. However, the structure of these compounds has not been reported yet. They were considered as

derivatives of the β-$Ca_3(PO_4)_2$ structure with the standard polar space group *R*3*c* in some works, while there is evidence that the crystal structure of $Ca_8MgR(PO_4)_7$ could be centrosymmetric [9].

Therefore, the aim of the present paper is to clarify the crystal symmetry of $Ca_8MgR(PO_4)_7$ with *R* = La, Pr, Nd, Sm–Lu, and Y, and to determine the distribution of R^{3+} cations among the crystallographic sites of the structure. The latter information is important for designing and modifying the luminescence properties of these materials. In addition, we also found antiferroelectric high-temperature phase transitions in all these compounds, and investigated luminescence properties of $Ca_8MgEu(PO_4)_7$ prepared under different conditions.

2. Experimental section

$Ca_8MgR(PO_4)_7$ (*R* = La, Pr, Nd, Sm–Lu, and Y) were synthesized by a standard solid-state method in air. Stoichiometric amounts of MgO (99.0%), $NH_4H_2PO_4$ (99.999%), $Ca_3(PO_4)_2$ (99.0%), and R_2O_3 (Pr_6O_{11} or Tb_4O_7) (99.9%) were heated in alumina crucibles at 873 K for 12 h followed by annealing at 1323–1473 K for 30 h for four times (with grindings at every step; the total annealing time at 1323–1473 K was 120 h). In order to determine the influence of sample preparation conditions on Eu^{3+} distributions among positions of the β-$Ca_3(PO_4)_2$-type structure, synthesized $Ca_8MgEu(PO_4)_7$ (sample I) was annealed and cooled under different conditions: at 1003 K for 6 h followed by slow cooling from the annealing temperature to room temperature (RT) (sample II) and at 1243 K for 6 h followed by quenching from the annealing temperature to liquid nitrogen (sample III).

Powder X-ray diffraction (PXRD) patterns were collected at RT with a SIEMENS D500 Bragg-Brentano-type powder diffractometer equipped with an incident-beam quartz-monochromator (Cu$K_{\alpha1}$ radiation, λ = 1.5406 Å) and a BRAUN position-sensitive detector. Silicon was used as an external standard. PXRD data were collected from 10° to 140° in 2θ with a step of 0.01°. The Rietveld analysis was performed using the JANA2006 program package [47].

Synchrotron PXRD data for $Ca_8MgEu(PO_4)_7$ (samples II and III) were measured on a large Debye−Scherrer camera at the BL15XU beamline of SPring-8 [48, 49]. The intensity data were collected from 1° to 62° in 2θ with a step of 0.003°; the incident beam was monochromatized at λ = 0.65297 Å. The samples were packed into Lindemann glass capillaries (inner diameter 0.1 mm), which were rotated during the measurement. The absorption coefficients were also measured, and the Rietveld analysis was performed using JANA2006 [47].

Selected area electron diffraction (SAED) patterns of $Ca_8MgEu(PO_4)_7$ (sample I) from 293 to 1063 K were obtained using a Philips CM20 transmission electron microscope equipped with a double-tilt heating holder. Samples for transmission electron microscopy (TEM) were prepared by crushing powders in agate mortars and dispersing them in methanol. After treatment in an

ultrasonic bath to disperse crystallites, a few drops of the dispersion were placed on copper grids with a holey carbon film.

The second-harmonic generation (SHG) response of powder samples was measured in a reflection mode. A Q-switch pulsed Nd:YAG laser operating at λ_ω = 1064 nm was used as the radiation source with a repetition rate of 4 impulses per second and a duration of impulses of about 12 ns. The experimental set-up was described elsewhere. The optical nonlinearity of the materials was evaluated relative to an α-quartz reference (polycrystalline α-SiO_2 with 3–5 μm particles size), $I_{2\omega}/I_{2\omega}(SiO_2)$. In fine powders, $I_{2\omega}/I_{2\omega}(SiO_2)$ is a quadratic function of spatially averaged components of the optical nonlinearity tensor [50]. The incident beam peak power was about 0.1 MW on a spot of 3-mm diameter on the surface of the sample. Taking into account that $I_{2\omega}/I_{2\omega}(SiO_2)$ should ideally be zero in centrosymmetric media we used it as an indicator of the presence or absence of the center of symmetry in our materials.

Differential scanning calorimetry (DSC) measurements were performed on a NETZSCH DSC 204 F1 calorimeter from 303 to 873 K (heating/cooling rate was 10 K/min) in a nitrogen flow (40 ml/min).

Electrical conductivity (σ), dielectric permittivity (ε), and dielectric loss tangent (tagδ) were measured on a Novocontrol Beta-N impedance-analyzer in a ProboStat measuring cell using the double-contact method in a frequency range of 10 Hz-1 MHz on heating with 2 K/min between 290 and 1200 K; ceramic pellets were 5-6 mm in diameter and 1.5-2 mm in height. A platinum paste was put on flat surfaces of pellets and heated to give Pt electrodes. The density of ceramic samples was above 90 % of the theoretical density, and a typical particle size was about 20-30 μm.

Photoluminescence emission (PL) and photoluminescence excitation (PLE) spectra were recorded on a Lot-Oriel MS-257 spectrometer equipped with a Marconi CCD detector and 150WXe arc as an excitation source. Photoluminescence spectra of all samples were measured under nearly the same conditions to reduce an error. All measurements were performed at RT and corrected for the sensitivity of the spectrometer.

3. Results and discussion

3.1. SHG, DSC, and dielectric measurements

Very weak SHG response (< 0.1) was detected in all $Ca_8Mg\mathit{R}(PO_4)_7$ (*R* = La, Pr, Nd, Sm–Lu, and Y); this fact strongly suggests centrosymmetric crystal structures.

Temperature dependencies of ε and tanδ at different frequencies are given in Figs. 1 and 2 for some $Ca_8Mg\mathit{R}(PO_4)_7$ compounds. Similar behavior of $\varepsilon(T)$ and tan$\delta(T)$ was observed for other samples. As shown in Fig. 1, all $\varepsilon(T)$ curves demonstrate a characteristic maximum at a certain

temperature depending on the R^{3+} cation. The temperature position of the dielectric anomalies does not depend on frequency. Such an anomaly can be attributed either to a ferroelectric [5-7] or an antiferroelectric phase transition [8, 9]. The absence of any anomalies on the tanδ(T) curves (Fig. 2) allows us to classify the phase transition as an antiferroelectric phase transition. Thus, the presence of an antiferroelectric phase transition supports the results of the SHG studies that the crystal structures of all $Ca_8MgR(PO_4)_7$ compounds are centrosymmetric.

Fig. 3 displays a fragment of typical heating/cooling DSC curves for some $Ca_8MgR(PO_4)_7$. DSC anomalies are observed whose positions agree well with the dielectric constant anomalies. DSC curves indicate the presence of only one peak (on heating) for each sample. Phase transition temperatures lie in the range from 705 to 862 K. Endothermic (on heating) and exothermic (on cooling) effects with noticeable hysteresis suggest first-order reversible phase transitions. The enthalpy (ΔH values) of the transitions and phase transition temperatures are summarized in Table S1 of the Supporting information.

3.2. PXRD and SAED studies

PXRD patterns of $Ca_8MgR(PO_4)_7$ (R = La, Pr, Nd, Sm–Lu, and Y) were similar to those of other β-$Ca_3(PO_4)_2$-type compounds. Indexing results and lattice parameters have been reported in the Powder Diffraction Files, for example, a = 10.3600 Å and c = 37.0853 Å for $Ca_8MgEu(PO_4)_7$ (PDF Card 45-0551; Table S1 in Supporting Information). The lattice parameters monotonically increase from Lu to La (Fig. S1 in Supporting Information). The absence of any impurity reflections showed that R^{3+} and Mg^{2+} cations were completely incorporated into the β-$Ca_3(PO_4)_2$-type host lattice.

The [0001]*, [11$\bar{2}$0]*, [$\bar{1}$101]* and [10$\bar{1}$0]* SAED patterns of $Ca_8MgEu(PO_4)_7$ at RT are shown in Fig. 4, they were very similar to those of other β-$Ca_3(PO_4)_2$-type compounds [5, 51, 52]. All reflections on the SAED patterns could be indexed in a trigonal system with the lattice parameters determined from PXRD data.

The [11$\bar{2}$0]* diffraction pattern exhibited a rhombohedral shift of the reflection rows along $\boldsymbol{c}^*$ by $h\,c^*/3$. Reflections on the SAED patterns obeyed the following reflection conditions: $-h + k + l = 3n$ for $hkil$, $h + l = 3n$ and $l = 2n$ for $h\bar{h}0l$, $l = 3n$ for $hh\bar{2}\bar{h}l$, and $l = 6n$ for $000l$ (in the hexagonal axes). This fact suggested only one centrosymmetric space group, $R\bar{3}c$ (taking into account the results of the SHG and dielectric studies). The presence of reflections with $l = 3n$ ($n = 2m + 1$) for $000l$ on the [10$\bar{1}$0] diffraction pattern can be explained by multiple diffraction. Indeed, the intensities of these reflections were systematically lower than those with $l = 6n$ and on tilting the sample around the [$000l$] axis, these reflections further weakened and vanished. Moreover, these reflections with $l = 3n$ ($n = 2m + 1$) for $000l$ were not observed on the [11$\bar{2}$0]* diffraction pattern.

Heating of $Ca_8MgEu(PO_4)_7$ from 293 to 1063 K resulted in an evolution of the [10$\bar{1}$0]* SAED patterns. Intensities of the $hh\overline{2h}l$: $l = 3n$ and 000l: $l = 3n$ ($n = 2m + 1$) reflections decreased with increasing temperature and vanished at 1073 K (Fig. 5). The disappearance of $hh\overline{2h}l$: $l = 3n$ and 000l: $l = 3n$ ($n = 2m + 1$) reflections of $R\bar{3}c$ space group together with the SHG results indicates a phase transition from space group $R\bar{3}c$ to $R\bar{3}m$ with halving of the c lattice parameter. This fact supports the AFE nature of the phase transition [8] because unit-cell dimensions do not usually change during FE phase transitions [51, 52].

3.3. Crystal structure refinements of $Ca_8Mg\mathit{R}(PO_4)_7$

The first three reflections (012, 104, and 006) on PXRD patterns of $Ca_8Mg\mathit{R}(PO_4)_7$ were broadened in comparison with other reflections (Fig. 6), and background was fitted poorly in the 2θ range of 10–16°. For this reason, a part of the XPRD patterns from 10° to 16° was excluded during the structure refinements of $Ca_8Mg\mathit{R}(PO_4)_7$.

The structural data for the high-temperature β´-$Ca_9In(PO_4)_7$ phase [51] were used as a starting model for the refinements of the structures of $Ca_8Mg\mathit{R}(PO_4)_7$ in the $R\bar{3}c$ model. Mg^{2+} ions were placed at the M5 site. R^{3+} and Ca^{2+} ions were located at the M1 and M3 sites. The M2 position is absent in the $R\bar{3}c$ structure; however, we kept the same position notations as in the parent β-$Ca_3(PO_4)_2$-type structure]. At the first stage, the f curves for Ca^{2+} (in the M1 and M3 sites) and Mg^{2+} (M5 site) were used, and all the parameters of this model were refined. The analysis of the occupancies demonstrated (Table S1 of the Supporting information, $n_{f\text{-Ca}}$ and $n_{f\text{-Mg}}$) that the R^{3+} cations are distributed between the M1 and M3 sites in $Ca_8Mg\mathit{R}(PO_4)_7$ with R = La–Ho, and just in one M1 site for R = Er–Lu. The occupancy of the M5 site by Mg^{2+} was close to unity for R = Pr–Er and Yb (parameters a_i were close to 1/6) (Table S1 of the Supporting information) while the parameter a_i for the M5 site for R = La, Tm, and Lu was slightly larger than 1/6 indicating that a small amount of Ca^{2+} cations is located at the M5 site ($M5 = n\ Mg^{2+} + (1\text{-}n)\ Ca^{2+}$).

Two disordered elements exist in the $R\bar{3}c$ structure of $Ca_8Mg\mathit{R}(PO_4)_7$: 1) cation disordering at the M3 sites and 2) disordering of $P1O_4$ tetrahedra. The M3 and P1 positions in the $R\bar{3}c$ structure are located near the positions with the site symmetries 18d (1/2,0, 0) and 6a (0, 0, 1/4), respectively. However, the refinement of a model with M3 and P1 fixed at those special positions resulted in very large atomic displacement parameters, $U_{iso.} = 0.131(2)$ Å^2 for Ca^{2+} at M3 and $U_{iso.} = 0.181(6)$ Å^2 for P1 (in case of R = Eu). For this reason, the refinement of the structures of all $Ca_8Mg\mathit{R}(PO_4)_7$ was performed with a displacement of the phosphorus atoms at the P1 site from the 6a special position to a half-occupied special position (site symmetry 12c) and a displacement of the M3 positions with the site symmetry 18d to a half-occupied position with site symmetry 36f.

At the second stage, the distribution of the R^{3+} cations between the *M*1 and *M*3 sites in the $Ca_8MgR(PO_4)_7$ structures was refined considering their multiplicities (*M*1 = *n* Ca^{2+} + (1-*n*) R^{3+} and *M*3 =*n* Ca^{2+} + (0.5-*n*) R^{3+}). For the samples with *R* = Er–Lu, the refined occupancy for the *M*3 site, n_{R3}, was close to 0. Thus, n_{R3} was fixed at 0 and n_{R1} was fixed at 1/6 in the last stage of the structure refinements of $Ca_8MgR(PO_4)_7$ with *R* = Er–Lu and Y.

The reliability factors R_{all} and R_p showed a good agreement between experimental and calculated PXRD patterns. As an example, Fig. 7 displays a fragment of the observed, calculated, and difference PXRD patterns of $Ca_8MgEu(PO_4)_7$ (sample I). Other numerical characteristics illustrating the quality of the structure refinements are presented in Table S1 of Supporting Information. The fractional atomic coordinates, isotropic atomic displacement parameters, and cation occupancies for $Ca_8MgR(PO_4)_7$ are listed in Table S2 of Supporting Information. The main interatomic distances for $Ca_8MgR(PO_4)_7$ are listed in Table S3 of Supporting Information.

Fig. 8 shows that there is a correlation between the size of the site, the cation radius, and the occupation factor: the small cations (Er-Lu) occupy only the small *M*1 site, the largest ones (La–Pr) showed a strong tendency to preferably occupy the large *M*3 site, whereas other cations (Nd–Ho) occupy both the *M*1 and *M*3 sites. In $Ca_9R(AO_4)_7$ (*R* = Tb–Lu; *A* = V [12] and P [23]) the *M*3 site is occupied only by Ca^{2+} for *A* = V and by Ca^{2+} and R^{3+} cations for *A* = P, whereas this site is occupied only by Ca^{2+} ions for *R* = Er–Lu in $Ca_8MgR(PO_4)_7$. In most of $Ca_8MgR(PO_4)_7$ compounds (except for *R* = La, Tm, and Lu), the *M*5 site is occupied only by Mg^{2+} ions (Table S2 of the Supporting information) in comparison with $Ca_9R(VO_4)_7$ [12] and $Ca_9R(PO_4)_7$ [23] (*R* = Tb–Lu) where R^{3+} cations partially occupy the *M*5 site. In $Ca_9R(VO_4)_7$ [20-22] and $Ca_9R(PO_4)_7$ [23] (*R* = La and Pr–Gd), the *M*5 site is occupied only by Ca^{2+} ions. Thus, the small Mg^{2+} ions preferably occupy the *M*5 site, prohibiting the location of R^{3+} ions in this site for all compounds $Ca_8MgR(PO_4)_7$.

Fig. 9 shows two neighboring *A* columns of the β-$Ca_3(PO_4)_2$-type structure with vacant *M*4 and *M*6 sites in the ferroelectric *R*3*c* phase and in idealized paraelectric $R\bar{3}m$ and antiferroelectric $R\,\bar{3}\,c$ phases with ordered $P1O_4$ tetrahedra. Note that in the average paraelectric and antiferroelectric phases, $P1O_4$ tetrahedra are disordered as mentioned before. Two neighboring *A* columns along the 3-fold axis in the antiferroelectric phase could have opposite orientations of $P1O_4$ tetrahedra (Fig. 9*c*) while $P1O_4$ tetrahedra are oriented in one direction in the ferroelectric phase (Fig. 9*b*) and make a certain contribution into ferroelectric and nonlinear optical properties. The phase transition from the antiferroelectric phase into the paraelectric one could be accompanied by a rotation of half of the $P1O_4$ tetrahedra. The *M*1 and *M*2 sites (site symmetry

18*b*) of the ferroelectric *R*3*c* phase are combined into one position with site symmetry 36*f* in the antiferroelectric phase $R\bar{3}c$.

3.4. Crystal structure refinements of $Ca_8MgEu(PO_4)_7$ samples prepared under different annealing and cooling conditions

The structural data for $Ca_8MgEu(PO_4)_7$ (sample I) were used as a starting model for refinements of crystal structures of $Ca_8MgEu(PO_4)_7$ (samples II and III) using synchrotron PXRD data. The reliability factors R_{all} and R_p showed a good agreement between experimental and calculated synchrotron PXRD patterns. Other numerical characteristics illustrating the quality of the structure refinements are presented in Table 1. The fractional atomic coordinates, isotropic atomic displacement parameters, and cation position occupancies for both $Ca_8MgEu(PO_4)_7$ samples are listed in Table S4 of the Supporting information, and main interatomic distances - in Table S5 of the Supporting information.

The Rietveld analysis of laboratory and synchrotron PXRD patterns reveals that preparation conditions practically do not affect the distribution of Ca^{2+} and Eu^{3+} cations among the structure positions. In accordance with Tables S2 and S4 of the Supporting information, the determined occupancy of *M*1 and *M*3 by Eu^{3+} cations lies in the range from 4.05 atoms (0.1123×36) to 4.50 atoms (0.1251×36) for the *M*1 position, and from 1.50 atoms (0.0416×36) to 1.95 atoms (0.0543×36) for the *M*3 position.

3.5. Luminescent properties of Eu^{3+}-containing samples

PLE and PL spectra of $Ca_8MgEu(PO_4)_7$ (sample I) are shown in Fig. 10. The PLE spectrum consists of intraconfigurational $4f^6$–$4f^6$ transitions of Eu^{3+} in the host lattice in the 310–500 nm region and a broad band in the 250–310 nm region. The broad excitation band is attributed to the O(2*p*)–Eu^{3+} charge transfer (CT) transition. The most intense Eu^{3+} 4*f*–4*f* excitations can be attributed to the $^7F_0 \rightarrow {}^5L_6$ transitions.

PL spectra of $Ca_8MgEu(PO_4)_7$ samples are shown in Fig. 10*b* and Fig. 11 after excitation at the $^7F_0 \rightarrow {}^5L_6$ transition of Eu^{3+} located at 395 nm. PL spectra in the spectral range from 570 to 650 nm demonstrate the typical red emitting features of Eu^{3+}, including $^5D_0 \rightarrow {}^7F_J$ (J = 0–4) emissions (Fig. 10*b*). $^5D_0 \rightarrow {}^7F_2$ forced electric dipole transition at ~ 615 nm is dominant and indicates that the site symmetry of the Eu^{3+} position possesses no inversion centre [54-55]. Emission wavelengths of these 4f-4f transitions are only moderately influenced by the environment of the lanthanide ions since the partially filled 4f shell is well shielded by the filled 5s and 5p orbitals. The $I(^5D_0 \rightarrow {}^7F_2)/I(^5D_0 \rightarrow {}^7F_1)$ ratio is often referred to as the asymmetry ratio [56]. For $Ca_8MgEu(PO_4)_7$ samples prepared under the different conditions, the values of this

ratio at RT are in the range of 4.24-4.27, in agreement with other β-$Ca_3(PO_4)_2$-based materials [24, 57-59] except for $Ca_{19}Mg_2(PO_4)_{14}$:Eu^{3+} ($I(^5D_0 \rightarrow {}^7F_2)/I(^5D_0 \rightarrow {}^7F_1)$ = 7.0) [33]. The high values of this ratio indicate that the local symmetry around Eu^{3+} cations is non-centrosymmetric. Moreover, the multiple splitting of the $^5D_0 \rightarrow {}^7F_1$ transition and the unusually high intensity of the $^5D_0 \rightarrow {}^7F_4$ transition (Fig. 10*b*) also originate from the low symmetry of the oxygen environment of the Eu^{3+} cations [60].

Fig. 11 shows parts of PL spectra of $Ca_8MgEu(PO_4)_7$ (samples I, II, and III) in the range of the $^5D_0 \rightarrow {}^7F_0$ and $^5D_0 \rightarrow {}^7F_2$ transitions of Eu^{3+}. The $^5D_0 \rightarrow {}^7F_0$ transition in the region 575–582 nm deserves the special attention. Since this transition is forbidden, both for electric and magnetic dipole interactions, the intensity can be very low or even non-observable. Yet, for C_1 symmetry the transition is induced, so a peak can be expected at that position. As splitting of the initial and final level, both characterized by $J = 0$, is not possible, the number of bands observed for the $^5D_0 \rightarrow {}^7F_0$ transition on PL spectra indicates the number of non-equivalent sites for the luminescent Eu^{3+} ions. The emission intensities for samples I, II, and III were slightly different. It is difficult to give an unambiguous reason for this observation. It could be caused either by the normalization process of the spectra or by a tiny, but observable, difference in the occupation factors (the amount of Eu^{3+} at the *M*1 site decreases from sample III to sample I to sample II).

Benhamou et al. [57] gave a summary of the relationship between distributions of Eu^{3+} cations among sites of the β-$Ca_3(PO_4)_2$-type structure (in $Ca_9Eu(PO_4)_7$) and its optical properties. The energy positions of $^5D_0 \rightarrow {}^7F_0$ bands for non-equivalent Eu^{3+} centers were related to the mean length of Eu–O bonds, $^5D_0 \rightarrow {}^7F_2/{}^5D_0 \rightarrow {}^7F_1$ intensity ratio and lifetimes of the $^5D_0 \rightarrow {}^7F_0$ emission. The $^5D_0 \rightarrow {}^7F_0$ transition shifted toward shorter wavelengths (higher energy) and the emission lifetime decreased with increasing Eu–O distances and distortion of the Eu^{3+} oxygen environment. In accordance with these relations, three bands in the region 575–582 nm observed for the $^5D_0 \rightarrow {}^7F_0$ transition on the $Ca_9Eu(PO_4)_7$ PL spectrum [57, 61] were associated with the Eu^{3+} cation occupation of *M*3, *M*1 and *M*2 sites of the β-$Ca_3(PO_4)_2$ (*R*3*c*) structure, respectively. In contrast to other compounds [24, 26, 57-59] we observe only one peak for all $Ca_8MgEu(PO_4)_7$ samples (Fig. 11*a*), the local environment of the Eu^{3+} ions probably remains the same over the whole crystal [62]. The position and the linewidth of the $^5D_0 \rightarrow {}^7F_0$ band practically does not change when changing the annealing and cooling conditions (~579 nm). A similar picture is observed for positions and linewidth of the $^5D_0 \rightarrow {}^7F_2$ bands (Fig. 11*b*).

The point group of β-$Ca_3(PO_4)_2$ is C_{3v}. However, the *M*1, *M*2, and *M*3 sites in the β-$Ca_3(PO_4)_2$-type structure have C_1 symmetry. For example, the *M*–O distances in $Ca_9Eu(PO_4)_7$ structure vary from 2.240 Å to 2.860 Å, from 2.320 Å to 2.780 Å, from 2.330 Å to 2.880 Å for the $M1O_8$, $M2O_8$, and $M3O_8$ polyhedra, respectively [57]. The $M3O_8$ polyhedron has the longest average

*M*3–O bond length ($d_{<Eu3-O>}$=2.577; $d_{<Ca3-O>}$=2.602 Å) and the largest distortion, or the difference between the shortest and the longest bond lengths, observed for the $Eu3O_8$ polyhedron (Δ=22.9 %). The $Ca_9Eu(PO_4)_7$ structure refinement shows that Eu^{3+} cations occupy *18-fold M*1–*M*3 positions of the β-$Ca_3(PO_4)_2$ (*R*3*c*) structure with the ratio Eu1:Eu2:Eu3=0.159:0.107:0.068 [57]. The determined occupancies of *M*1+*M*2 and *M*3 by Eu^{3+} cations are 4.8 atoms ((0.159+0.107)×18) and 1.2 atoms (0.068×18).

The substitution of Mg^{2+} for Ca^{2+} in $Ca_9Eu(PO_4)_7$ with the formation of $Ca_8MgEu(PO_4)_7$ leads to a significant increase of the amount of Eu^{3+} at the *M*3 site (1.7 atoms (0.0461×36) and to a decrease of the occupation of *M*1 (*36-fold*) by Eu^{3+} (4.3 atoms ((0.1205)×36) of the $R\bar{3}c$ structure (with Tables S2 and S4 of the Supporting information). Moreover, the substitution of Mg^{2+} for Ca^{2+} results in the decrease of the difference between the average *M*–O bond length in the $M1O_9$ and $M3O_8$ polyhedra ($d_{<M1-O>}$ = 2.463-2.466; $d_{<M3-O>}$ = 2.538-2.547 Å) and the increase of the distortion of the $M3O_8$ polyhedra from Δ = 22.9 % in $Ca_9Eu(PO_4)_7$ to Δ = 23.7-23.9 % in $Ca_8MgEu(PO_4)_7$ (Tables S3 and S5 of the Supporting information).

4. Conclusions

We used a combination of second-harmonic generation, dielectric measurements, electron diffraction, and structural analysis to show that $Ca_8MgR(PO_4)_7$ (*R* = La, Pr, Nd, Sm–Lu, and Y) crystallize in centrosymmetric space group $R\bar{3}c$ in comparison with the parent compounds β-$Ca_3(PO_4)_2$ and $Ca_9R(PO_4)_7$ (*R* = La, Pr, Nd, Sm–Lu, and Y), which adopt a polar *R*3*c* structure. Reversible antiferroelectric first-order phase transitions were detected by dielectric and differential scanning calorimetry measurements and electron diffraction. We found that R^{3+} cations are distributed between the *M*1 and *M*3 sites in a systematic way depending on the size of R^{3+}; this information could be helpful in designing luminescent properties of these materials. We showed that synthesis conditions of $Ca_8MgEu(PO_4)_7$ do not affect the distribution of Ca^{2+} and Eu^{3+} cations between the structure sites and do not change its luminescent properties. All $Ca_8MgEu(PO_4)_7$ phosphors emit intense red light dominated by the $^5D_0$ – $^7F_2$ transition at ~614 nm. In contrast to other β-$Ca_3(PO_4)_2$-type compounds, only one band is observed for the $^5D_0 \rightarrow {}^7F_0$ transition.

Acknowledgements

This work was supported by Russian Science Foundation (Grant 16-13-10340). J.H. and V.A.M. are grateful for support by FWO Flanders Research Foundation under project G039211N. We thank Dr. S. S. Khasanov for collecting laboratory PXRD data. The synchrotron radiation

experiments were performed at the NIMS synchrotron X-ray station at SPring-8 with the approval of the Japan Synchrotron Radiation Research Institute (Proposal Number: 2015A4502).

References

[1] B. Dickens, L. W. Schroeder, W. E. Brown, Crystallographic studies of the role of Mg as a stabilizing impurity in β-$Ca_3(PO_4)_2$. The crystal structure of pure β-$Ca_3(PO_4)_2$, J. Solid State Chem. 10 (1974) 232-248.

[2] L. Jiang, R. Pang, D. Li, W. Sun, Y. Jia, H. Li, Fu J., Ch. Li, S. Zhang, Tri-chromatic white-light emission from a single-phase $Ca_9Sc(PO_4)_7$:Eu^{2+}, Tb^{3+}, Mn^{2+} phosphor for LED applications, Dalton Trans. 44 (2015) 17241-17250.

[3] T. Nakajima, T. Tsuchiya, Plant habitat-conscious white light emission of Dy^{3+} in whitlockite-like phosphates: reduced photosynthesis and inhibition of bloom impediment, ACS Appl. Mater. Interfaces 7 (2015) 21398−21407.

[4] S. Sun, Z. Lin, L. Zhang, Y. Huang, G.Wang, Growth and spectral properties of a new nonlinear laser crystal of Nd^{3+}:$Ca_9Y_{0.5}La_{0.5}(VO_4)_7$, J. Alloys Compd. 551 (2013) 229-232.

[5] B. I. Lazoryak, O. V. Baryshnikova, S.Yu. Stefanovich, A.P. Malakho, V. A. Morozov, A. A. Belik, I. A. Leonidov, O. N. Leonidova, G. Van Tendeloo, Ferroelectric and ionic-conductive properties of nonlinear-optical vanadate, $Ca_9Bi(VO_4)_7$, Chem. Mater. 15 (2003) 3003-3010.

[6] O. L. Vorontsova, A. P. Malakho, V. A. Morozov, S. Yu. Stefanovich, B. I. Lazoryak, Ferroelectric and nonlinear optical properties of $Ca_{9-x}Cd_xBi(VO_4)_7$ vanadates, Russ. J. Inorg. Chem. 49 (2004) 1932-1942.

[7] O. V. Baryshnikova, A. P. Malakho, K. K. Kobyletskii, A. A. Fursina, O. N. Leonidova, V. A. Morozov, I. A. Leonidov, S. Yu. Stefanovich, B. I. Lazoryak, Ferroelectric solid solutions in the $Ca_3(VO_4)_2$-$BiVO_4$ system, Russ. J. Inorg. Chem. 50 (2005) 823-832.

[8] S. Yu. Stefanovich, A. A. Belik, M. Azuma, M. Takano, O. V. Baryshnikova, V. A. Morozov, B. I. Lazoryak, O. I. Lebedev, G. Van Tendeloo, Antiferroelectric phase transition in $Sr_9In(PO_4)_7$, Phys. Rev. B 70 (2004) 172103.

[9] A. V. Teterskii, S. Yu. Stefanovich, B. I. Lazoryak, D. A. Rusakov, Whitlockite solid solutions $Ca_{9-x}M_xR(PO_4)_7$ (x = 1, 1.5; M = Mg, Zn, Cd; R = Ln, Y) with antiferroelectric properties, Russ. J. Inorg. Chem. 52 (2007) 308–314.

[10] A. Benarafa, M. Kacimi, G. Coudurier, M. Ziyad, Characterisation of the active sites in butan-2-ol dehydrogenation over calcium–copper and calcium–sodium–copper phosphates, Appl. Catal. A 196 (2000) 25-35.

[11] D. E. Wagner, K. M. Eisenmann, A. L. Nestor-Kalinoski, S. B. Bhaduri, A microwave-assisted solution combustion synthesis to produce europium-doped calcium phosphate nanowhiskers for bioimaging applications, Acta Biomaterialia 9 (2013) 8422-8432.

[12] A. A. Belik, S. V. Grechkin, L. O. Dmitrienko, V. A. Morozov, B. I. Lazoryak, Crystal structures of double vanadates $Ca_9R(VO_4)_7$. IV. R = Er, Tm, Yb, and Lu, Crystallogr. Rep. 45 (2000) 896-901.

[13] V. N. Golubev, B. N. Viting, O. B. Dogadin, B. I. Lazoryak, $Ca_9M(PO_4)_7$ (M = Al, Fe, Cr, Ga, Sc, Sb, In) binary phosphates, Rus. J. Inorg. Chem. 35 (1990) 3037-3041.

[14] L.W. Schroeder, B. Dickens, W.E. Brown, Crystallographic studies of the role of Mg as a stabilizing impurity in β-$Ca_3(PO_4)_2$. II. Refinement of Mg-containing β-$Ca_3(PO_4)_2$, J. Solid State Chem. 22 (1977) 253-262.

[15] A. A. Belik, O. V. Yanov, B. I. Lazoryak, Synthesis and crystal structure of $Ca_9Cu_{1.5}(PO_4)_7$ and reinvestigation of $Ca_{9.5}Cu(PO_4)_7$, Mater. Res. Bull. 36 (2001) 1863-1871.

[16] A. G. Nord, Incorporation of divalent metals in whitlockite-related beta-$Ca_3(PO_4)_2$, N. Jb. Miner. Mh. 11 (1983) 489-497.

[17] V. A. Morozov, I. A. Presnyakov, A. A. Belik, S. S. Khasanov, B. I. Lazoryak, Crystal structures of triple calcium, magnesium, and alkali metal phosphates $Ca_9MgM(PO_4)_7$ (M = Li, Na, K), Crystallogr. Rep. 42 (1997) 758-769.

[18] A. A. Belik, V. B. Gutan, L. N. Ivanov, B. I. Lazoryak, Synthesis, structure, and luminescence properties of $Ca_9MnM(PO_4)_7$ (M = Li, Na, K), Rus. J. Inorg. Chem. 46 (2001) 785-792.

[19] A. A. Belik, F. Izumi, T. Ikeda, A. P. Malakho, B. I. Lazoryak, Strontium phosphates with beta-$Ca_3(PO_4)_2$-type structures: $Sr_9NiLi(PO_4)_7$, $Sr_{9.04}Ni_{1.02}Na_{0.88}(PO_4)_7$, and $Sr_{9.08}Ni_{1.04}K_{0.76}(PO_4)_7$, J. Mater. Chem. 12 (2002) 3803-3808.

[20] A. A. Belik, V. A. Morozov, S. S. Khasanov, B. I. Lazoryak, Crystal structures of double vanadates $Ca_9R(VO_4)_7$. I. R = La, Pr, and Eu, Crystallogr. Rep. 42 (1997) 751-757.

[21] A. A. Belik, V. A. Morozov, R. N. Kotov, S. S. Khasanov, B. I. Lazoryak, Crystal structure of double vanadates $Ca_9R(VO_4)_7$. II. R = Tb, Dy, Ho, and Y, Crystallogr. Rep., 2000, 45, 389-394.

[22] A. A. Belik, V. A. Morozov, S. V. Grechkin, S. S. Khasanov, B. I. Lazoryak, Crystal structures of double vanadates, $Ca_9R(VO_4)_7$. III. R = Nd, Sm, Gd, or Ce, Crystallogr. Rep. 45 (2000) 728-733.

[23] A. Bessiere, R. A. Benhamou, G. Walleza, A. Lecointrea, B. Viana, Site occupancy and mechanisms of thermally stimulated luminescence in $Ca_9Ln(PO_4)_7$ (Ln = lanthanide), Acta Materialia 60 (2012) 6641–6649.

[24] D. V. Deyneko, V. A. Morozov, J. Hadermann, A. E. Savon, D. A. Spassky, S. Yu. Stefanovich, A. A. Belik, B. I. Lazoryak, A novel red $Ca_{8.5}Pb_{0.5}Eu(PO_4)_7$ phosphor for light emitting diodes application, J. Alloys Compd. 647 (2015) 965–972.

[25] Y. Huang, W. Zhao, Y. Cao, K. Jang, S. H. Lee, E. Cho, S.-S. Yi, Photoluminescence of Eu^{3+}-doped triple phosphate $Ca_8MgR(PO_4)_7$ (R=La, Gd, Y), J. Solid State Chem. 181 (2008) 2161– 2164.

[26] Y. Huang, C. Jiang, Y. Cao, L. Shi, H. J. Seo, Luminescence and microstructures of Eu^{3+} doped in triple phosphate $Ca_8MgR(PO_4)_7$ (R = La, Gd, Y) with whitlockite structure, Mat. Res. Bull. 44 (2009) 793–798.

[27] Y. Huang, H. Ding, K. Jang, E. Cho, H.S. Lee, M. Jayasimhadri, S.-S. Yi, Luminescence properties of triple phosphate $Ca_8MgGd(PO_4)_7$:Eu^{2+} for white light-emitting diodes, J. Phys. D: Appl. Phys. 41 (2008) 095110.

[28] J. Zhang, Yu. Wang, Y. Huang, Photoluminescence of Tb^{3+} and Mn^{2+} activated $Ca_8MgGd(PO_4)_7$ under vacuum ultraviolet excitation, Optical Materials 33 (2011) 1325-1330.

[29] Y. N. Xue, F. Xiao, Q. Y. Zhang, A red-emitting $Ca_8MgLa(PO_4)_7$: Ce^{3+}, Mn^{2+} phosphor for UV-based white LEDs application, Spectrochimica Acta A 78 (2011) 1445–1448.

[30] J. Zhang, C. Jiang, Photoluminescence properties of emission-tunable $Ca_8MgLa(PO_4)_7$: Eu^{2+}, Mn^{2+} phosphors for white LEDs, Optical Materials Express 4 (2014) 2102-2107.

[31] Z. W. Zhang, A. J. Song, M. Z. Ma, X. Y. Zhang, Y. Yue, R. P. Liu, A novel white emission in $Ca_8MgBi(PO_4)_7$: Dy^{3+} single-phase full-color phosphor, J. Alloys Compd. 601 (2014) 231–233.

[32] X. Mi, J. Sun, P. Zhou, H. Zhou, D. Song, K. Li, M. Shang, L. Jun, Tunable luminescence and energy transfer properties in $Ca_8MgLu(PO_4)_7$: Ce^{3+}, Tb^{3+}, Mn^{2+} phosphors, J. Mater. Chem. C 3 (2015) 4471-4481.

[33] G. Zhu, Z. Ci, Y. Shi, M. Que, Q. Wang, Y. Wang, Synthesis, crystal structure and luminescence characteristics of a novel red phosphor $Ca_{19}Mg_2(PO_4)_{14}:Eu^{3+}$ for light emitting diodes and field emission displays, J. Mater. Chem. C 1 (2013) 5960–5969.

[34] F. Y. Xie, Z. Y. Dong, D. W. Wen, J. Yan, J. X. Shi, J. Y. Shi, M. M. Wu, A novel pure red phosphor $Ca_8MgLu(PO_4)_7:Eu^{3+}$ for near ultraviolet white light-emitting diodes, Ceram. Int. 41 (2015) 9610–9614.

[35] Z. W. Zhang, Y. J. Ren, L. Liu, J. P. Zhang, Y. S. Peng, Synthesis and luminescence of Eu^{3+}-doped in triple phosphate $Ca_8MgBi(PO_4)_7$ with whitlockite structure, J. Lumin., 30 (2015) 1190-1194.

[36] Q. Long, C. Wang, Y. Y. Li, J. Y. Ding, Y. H. Wang, Synthesis and investigation of photo/cathodo luminescence properties of a novel green emission phosphor $Sr_8ZnLu(PO_4)_7:Eu^{2+}$, J. Alloys Compd. 671 (2016) 372-380.

[37] C. H. Huang, Y. C. Chen, T. M. Chen, T. S. Chan, H. S. Sheu, Near UV-pumped yellow-emitting $Sr_8MgSc(PO_4)_7:Eu^{2+}$ phosphor for white-light LEDs with excellent color rendering index, J. Mater. Chem. 21 (2011) 5645-5649.

[38] J. Zhang, Y. Wang, G. Chen, Y. Huang, Investigation on visible quantum cutting of Tb^{3+} in oxide hosts, J. Appl. Phys. 115 (2014) 093108.

[39] G. Zhu, Y. Wang, Q. Wang, X. Ding, W. Geng, Y. Shi, A novel white emitting phosphor of Dy^{3+} doped $Ca_{19}Mg_2(PO_4)_{14}$ for light-emitting diodes, J. Lumin. 154 (2014) 246–250.

[40] S. Y. Xin, G. Zhu, B. Wang, Z. F. Shao, The luminescent property and abnormal thermal quenching behavior of Pr^{3+} ions in novel red phosphor $Ca_{19}Mg_2(PO_4)_{14}:Pr^{3+}$, J. Lumin. 181 (2017) 455-458.

[41] G. Zhu, Z. P. Ci, Y. R. Shi, Y. H. Wang, Synthesis and photoluminescence properties of $Ca_{19}Mg_2(PO_4)_{14}:Sm^{3+}$ red phosphor for white light emitting diodes, Mater. Res. Bull. 55 (2014) 146–149.

[42] F. Y. Xie, J. H. Li, Z. Y. Dong, D. W. Wen, J. X. Shi, J. Yan, M. M. Wu, Energy transfer and luminescent properties of $Ca_8MgLu(PO_4)_7:Tb^{3+}/Eu^{3+}$ as a green-to-red color tunable phosphor under NUV excitation, RSC Adv. 5 (2015) 59830-59836.

[43] D. W. Wen, Z. Y. Dong, J. X. Shi, M. L. Gong, M. M. Wu, Standard white-emitting $Ca_8MgY(PO_4)_7:Eu^{2+}$, Mn^{2+} phosphor for white-light-emitting LEDs, ECS, Solid State Sci. Technol. 2 (2013) 178–185.

[44] J. Zhang, Z. Y. Zhai, Z. H. Hua, Investigations on luminescence of $Ca_8MgGd(PO_4)_7:Eu^{2+}$, Mn^{2+}, Yb^{3+}, Er^{3+}, Ho^{3+}, Tm^{3+} phosphors, Mater. Res. Bull. 74 (2016) 34–40.

[45] C. H. Huang, P. J. Wu, J. F. Leeb, T. M. Chen, $(Ca,Mg,Sr)_9Y(PO_4)_7:Eu^{2+}$, Mn^{2+}: Phosphors for white-light near-UV LEDs through crystal field tuning and energy transfer, J. Mater. Chem. 21 (2011) 10489-10495.

[46] X. Mi, J. Sun, P. Zhou, H. Zhou, D. Song, K. Li, M. Shang, L. Jun, Tunable luminescence and energy transfer properties in $Ca_8MgLu(PO_4)_7$: Ce^{3+}, Tb^{3+}, Mn^{2+} phosphors, J. Mater. Chem. C 3 (2015) 4471-4481.

[47] V. Petricek, M. Dusek, L. Palatinus, Crystallographic computing system JANA2006: General features, Z. Kristallogr. 229 (2014) 345-352.

[48] M. Tanaka, Y. Katsuya, A. Yamamoto, A new large radius imaging plate camera for high-resolution and high-throughput synchrotron x-ray powder diffraction by multiexposure method, Rev. Sci. Instrum. 79 (2008) 075106.

[49] M. Tanaka, Y. Katsuya, Y. Matsushita, O. Sakata, Development of a synchrotron powder diffractometer with a one-dimensional X-ray detector for analysis of advanced materials, J. Ceram. Soc. Jpn. 121 (2013) 287−290.

[50] S.K. Kurtz, T.T. Perry, A powder technique for the evaluation of nonlinear optical materials, J. Appl. Phys. 39 (1968) 3798-3813

[51] V.A. Morozov, A.A. Belik, S.Yu. Stefanovich, V.V. Grebenev, O.I. Lebedev, G. Van Tendeloo, B.I. Lazoryak, High-temperature phase transition in the whitlockite-type phosphate $Ca_9In(PO_4)_7$, J. Solid State Chem. 165 (2002) 278-288.

[52] B.I. Lazoryak, V.A. Morozov, A.A. Belik, S.Yu. Stefanovich, V.V. Grebenev, I.A. Leonidov, E.B. Mitberg, S.A. Davydov, O.I. Lebedev, G. Van Tendeloo, Ferroelectric phase transition in the whitlockite-type $Ca_9Fe(PO_4)_7$; crystal structure of the paraelectric phase at 923 K, Solid State Sci. 6 (2004) 185-195.

[53] R. D. Shannon, Revised effective ionic radii and systematic studies of interatomic distances in halides and chalcogenides, Acta Cryst. A 32 (1976) 751-767.

[54] R. J. Wiglusz, A. Bednarkiewicz, W. Strek, Role of the sintering temperature and doping level in the structural and spectral properties of Eu-doped nanocrystalline YVO_4, Inorg. Chem. 51 (2012) 1180-1186.

[55] P. Tanner, Some misconceptions concerning the electronic spectra of tri-positive europium and cerium, Chem. Soc. Rev. 42 (2013) 5090 – 5101.

[56] M. H. V. Werts, R. T. F. Jukes, J. W. Verhoeven, The emission spectrum and the radiative lifetime of Eu^{3+} in luminescent lanthanide complexes, Phys. Chem. Chem. Phys. 4 (2002) 1542-1548.

[57] R. A. Benhamou, A. Bessiere, G. Wallez, B. Viana, M. Elaatmani, M. Daoud, A. Zegzouti, New insight in the structure–luminescence relationships of $Ca_9Eu(PO_4)_7$, J. Solid State Chem. 182 (2009) 2319–2325.

[58] F. Du, Y. Nakai, T. Tsuboi, Y. Huang, H. J. Seo, Luminescence properties and site occupations of Eu^{3+} ions doped in double phosphates $Ca_9R(PO_4)_7$ (R = Al, Lu), J. Mater. Chem. 21 (2011) 4669–4678.

[59] F. Du, R. Zhu, Y. Huang, Y. Taob, H. J. Seo, Luminescence and microstructures of Eu^{3+}-doped $Ca_9LiGd_{2/3}(PO_4)_7$, Dalton Trans. 40 (2011) 11433–11440.

[60] R. A. S. Ferreira, S. S. Nobre, C. M. Granadeiro, H. I. S. Nogueira, L. D. Carlos, O. Malta, A theoretical interpretation of the abnormal $^5D_0 \rightarrow {}^7F_4$ intensity based on the Eu^{3+} local coordination in the $Na_9[EuW_{10}O_{36}]\cdot 14H_2O$ polyoxometalate, J. Lumin. 121 (2006) 561–567.

[61] B.I. Lazoriak, V.N. Golubev, R. Salmon, C. Parent, P. Hagenmuller, Distribution of Eu ions in whitlockite-type orthophosphates $Ca_{3-x}Eu_{2x/3}(PO_4)_2$, Eur. J. Solid State Inorg. Chem. 26 (1989) 455-463.

[62] G. Blasse, A. Bril, W.C. Nieuwpoort, On the Eu^{3+} fluorescence in mixed metal oxides Part I – The crystal structure sensitivity of thr intensity ratio of electric and magnetic dipole emission, J. Phys. Chem. Solids 27 (1966) 1587-1592.

Table 1 Crystallographic Data for $Ca_8MgEu(PO_4)_7$ samples (SG $R\bar{3}c$, Z = 6, and T = 293 K)

	Sample II	Sample III
Preparation conditions from $Ca_8MgEu(PO_4)_7$ (sample I)	at 1003 K followed by slow cooling to RT	at 1243 K followed by quenching to liquid N_2
Lattice parameters: a, Å	10.36157(6)	10.36191(7)
c, Å	37.09945(4)	37.1027(3)
Unit cell volume, Å^3	3449.45(4)	3449.97(4)
Calculated density, g/cm^3	3.35539(4)	3.35488(4)
Data Collection		
Radiation/ Wavelength λ, Å	Synchrotron / 0.65297	
Calc./exp. abs. coef. μ, mm^{-1}	4.046/2.23	4.044/1.85
F(000)	3384	
2θ range used, deg	6.161-37.608	6.335-39.555
2θ step scan, deg	0.003	
I_{max}	178240	174991
Number of points	10334	11123
Refinement		
Refinement	Rietveld	
Background function	Legendre polynomials, 20 terms	
No. of all reflections	388	450
No. of all refined parameters/ atomic parameters	64/36	64/36
R and R_w for Bragg reflections, %	2.38 and 3.36	3.42 and 4.45
R_P, R_{wP}, R_{exp}, %	2.10, 2.94, 0.76	2.40, 3.37, 0.77
Goodness of fit (ChiQ)	3.88	4.38
Max./min. residual density, e/Å^3	0.57/-0.28	0.68/-0.34
Selected crystal structure data		
Occupation of $M1$	$0.8877Ca^{2+}+0.1123Eu^{3+}$	$0.8749Ca^{2+}+0.1251Eu^{3+}$
Occupation of $M3$	$0.4457Ca^{2+}+0.0543Eu^{3+}$	$0.4584Ca^{2+}+0.0416Eu^{3+}$

Figure captions.

Fig. 1 Temperature dependencies of dielectric constant, $\varepsilon(T)$, for $Ca_8MgR(PO_4)_7$ with R = (a) Pr, (b) Tb, and (c) Lu.

Fig. 2 Temperature dependencies of dielectric loss tangent, tan $\delta(T)$, for $Ca_8MgR(PO_4)_7$ with R = (a) Pr, (b) Tb, and (c) Lu.

Fig. 3 A fragment of heating (solid lines) and cooling (dotted thick lines) DSC curves for some $Ca_8MgR(PO_4)_7$. Heating/cooling rate is 10 K/min.

Fig. 4 Selected area electron diffraction patterns along the main zone axes of $Ca_8MgEu(PO_4)_7$ (sample I) at room temperature.

Fig. 5 $[10\,\bar{1}\,0]^*$ electron diffraction patterns of $Ca_8MgEu(PO_4)_7$ (sample I) at different temperatures.

Fig. 6 Parts of laboratory XPRD patterns of $Ca_8MgR(PO_4)_7$ (R = La, Pr, Gd, and Lu) in the 2θ range of 10–20°. Indexes of the observed reflections are given.

Fig. 7 A fragment (16–64°) of observed, calculated, and difference laboratory PXRD patterns for $Ca_8MgEu(PO_4)_7$ (sample I). Tick marks denote the peak positions of possible Bragg reflections.

Fig. 8 Number of R^{3+} cations at the $M1$ and $M3$ sites in the whole unit cell in the structures of $Ca_8MgR(PO_4)_7$ (Z = 6) as a function of R^{3+} radii for 8-fold coordination, $r_{VIII}(R^{3+})$ [53].

Fig. 9 Two neighboring so-called A columns in the β-$Ca_3(PO_4)_2$-type structure with vacant $M4$ and $M6$ sites. The location of some $P1O_4$ tetrahedra is emphasized by the arrows. (b) Ferroelectric $R3c$ phase. (a) Paraelectric $R\bar{3}m$ and (c) antiferroelectric $R\bar{3}c$ phases; 'idealized' orientations of $P1O_4$ tetrahedra in these phases are shown because in the average structures, $P1O_4$ tetrahedra are highly disordered.

Fig. 10 (a) Room temperature photoluminescence excitation (λ_{em} = 615 nm) and (b) photoluminescence emission (λ_{ex} = 395 nm) spectra of $Ca_8MgEu(PO_4)_7$ (sample I). CT: charge transfer.

Fig. 11 Parts of room temperature photoluminescence emission spectra of $Ca_8MgEu(PO_4)_7$ (samples I, II, and III) for (a) $^5D_0 \rightarrow {}^7F_0$ and (b) $^5D_0 \rightarrow {}^7F_2$ transitions.

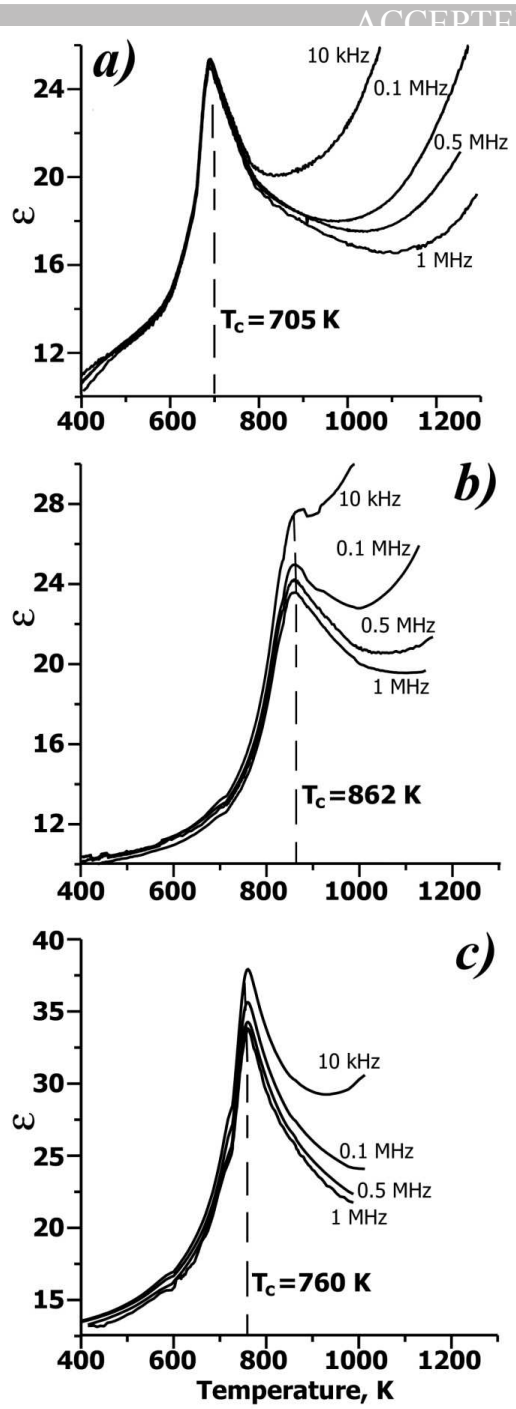

Fig. 1 Temperature dependencies of dielectric constant, $\varepsilon(T)$, for $Ca_8MgR(PO_4)_7$ with R = (a) Pr, (b) Tb, and (c) Lu.

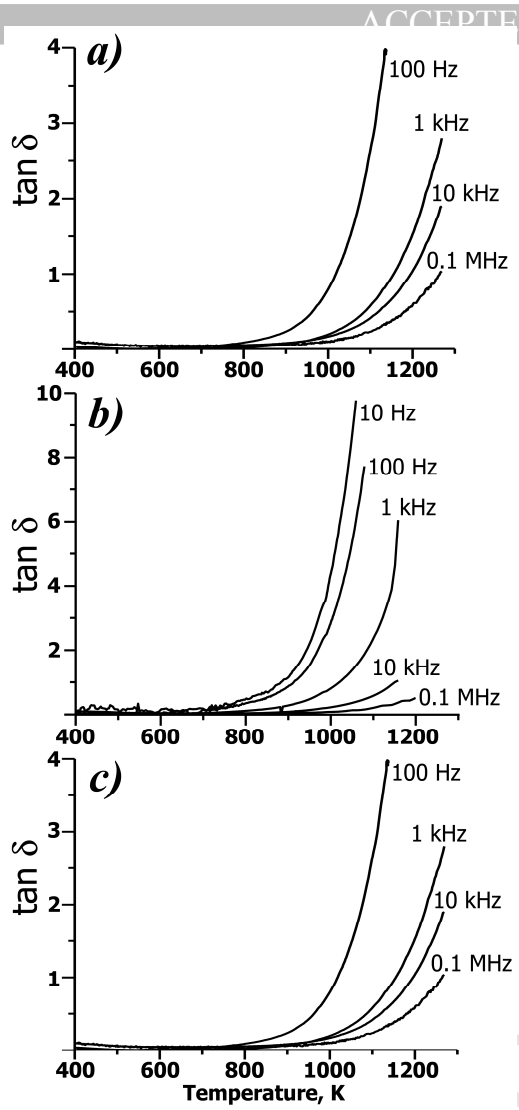

Fig. 2 Temperature dependencies of dielectric loss tangent, tan $\delta(T)$, for $Ca_8MgR(PO_4)_7$ with R = (a) Pr, (b) Tb, and (c) Lu.

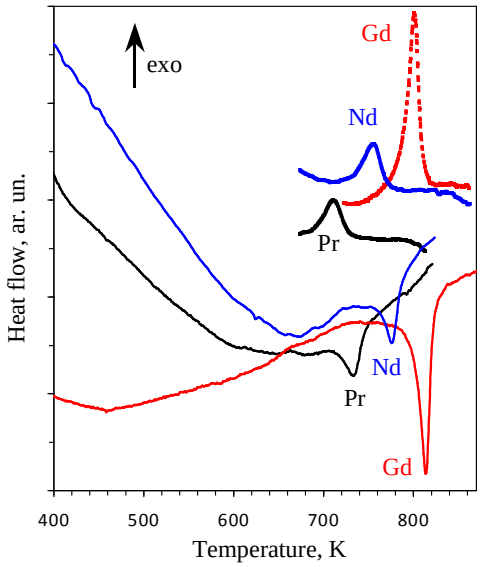

Fig. 3 A fragment of heating (solid lines) and cooling (dotted thick lines) DSC curves for some $Ca_8MgR(PO_4)_7$. Heating/cooling rate is 10 K/min.

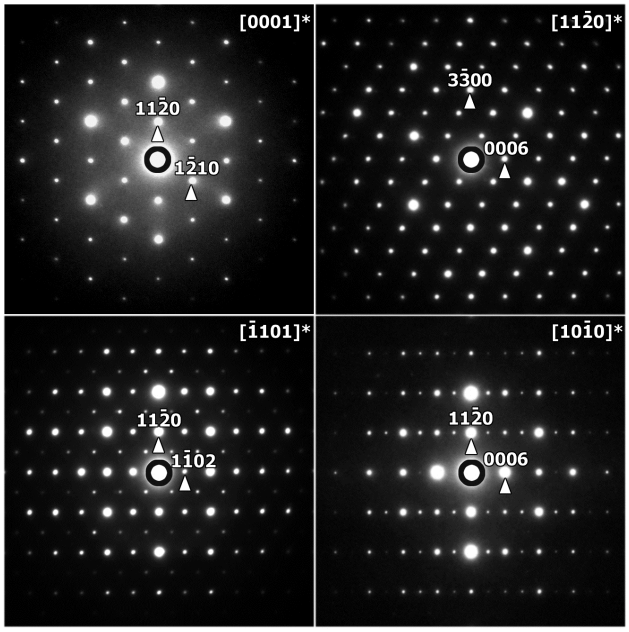

Fig. 4 Selected area electron diffraction patterns along the main zone axes of $Ca_8MgEu(PO_4)_7$ (sample I) at room temperature.

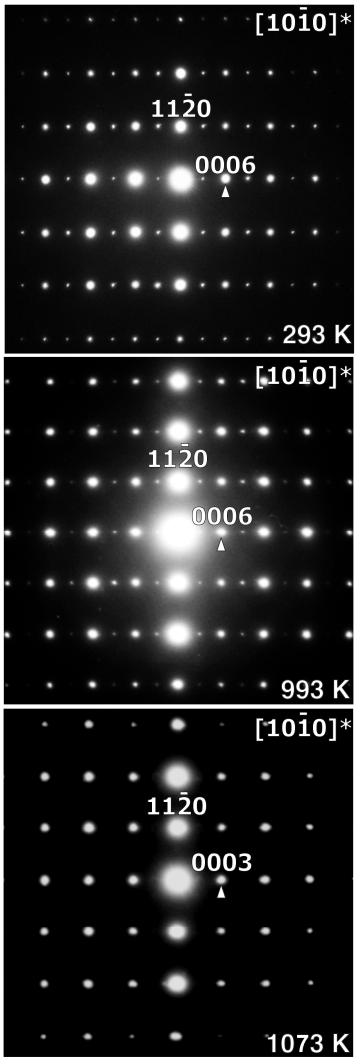

Fig. 5 [10 $\bar{1}$ 0]* electron diffraction patterns of $Ca_8MgEu(PO_4)_7$ (sample I) at different temperatures.

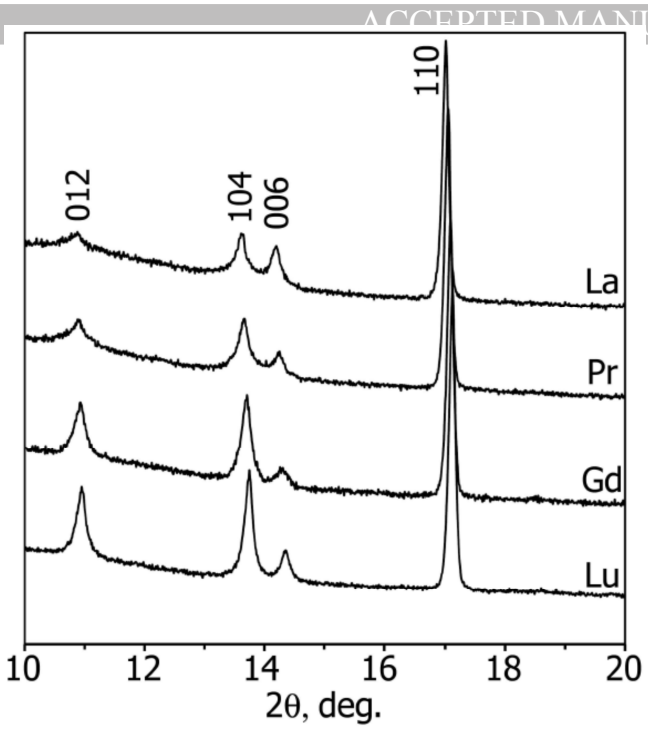

Fig. 6 Parts of laboratory XPRD patterns of $Ca_8MgR(PO_4)_7$ (R = La, Pr, Gd, and Lu) in the 2θ range of 10–20°. Indexes of the observed reflections are given.

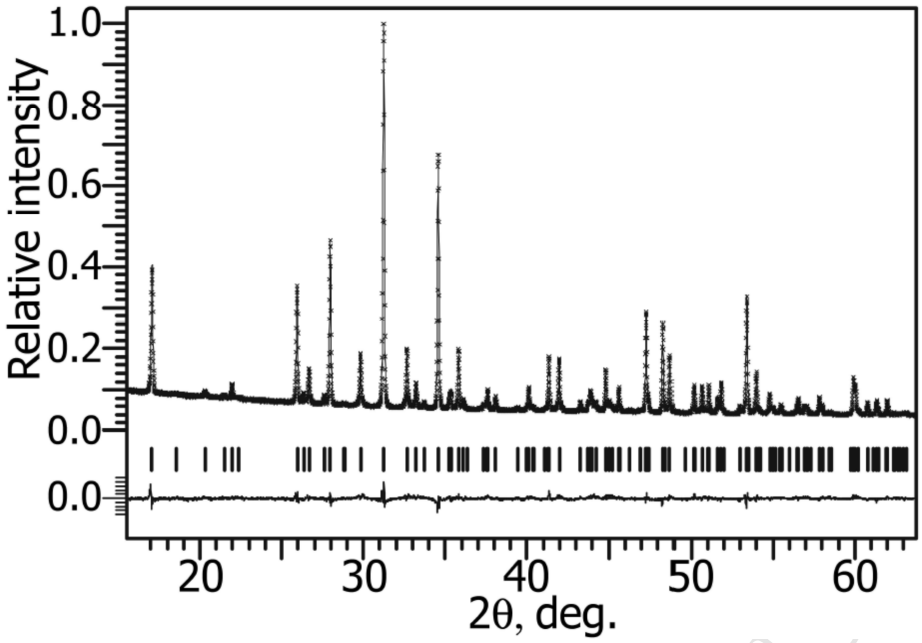

Fig. 7 A fragment (16–64°) of observed, calculated, and difference laboratory PXRD patterns for $Ca_8MgEu(PO_4)_7$ (sample I). Tick marks denote the peak positions of possible Bragg reflections.

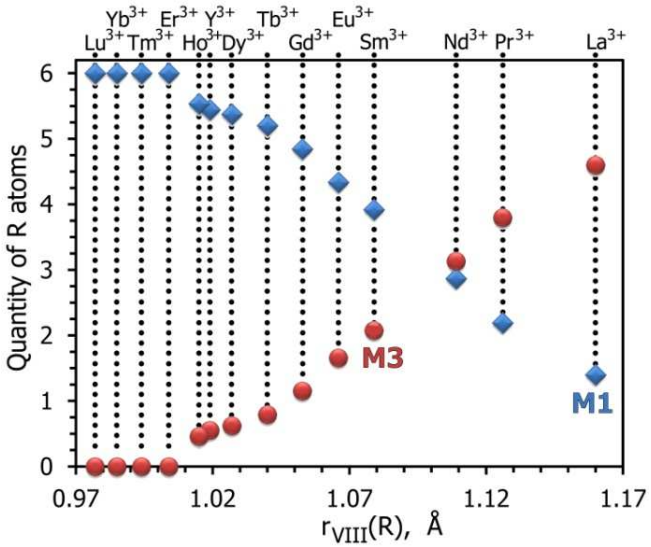

Fig. 8 Number of R^{3+} cations at the $M1$ and $M3$ sites in the whole unit cell in the structures of $Ca_8MgR(PO_4)_7$ (Z = 6) as a function of R^{3+} radii for 8-fold coordination, $r_{VIII}(R^{3+})$ [53].

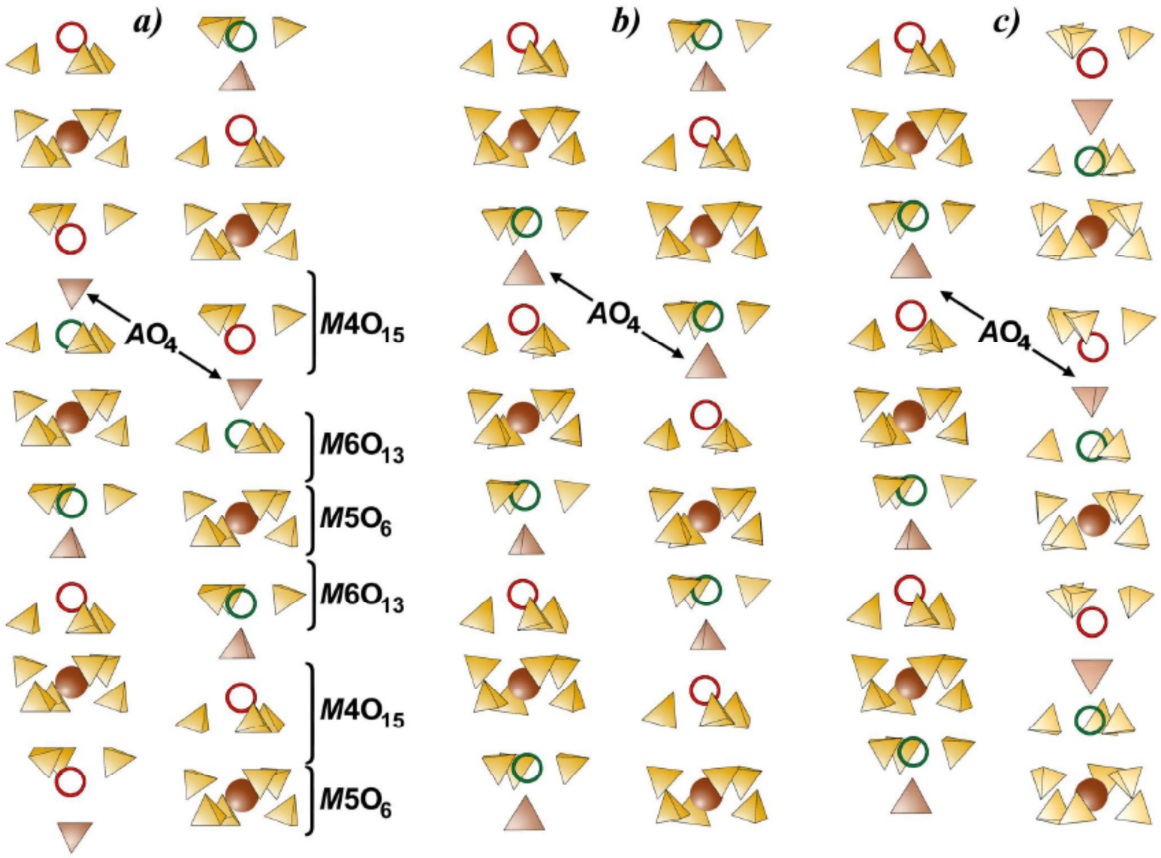

Fig. 9 Two neighboring so-called *A* columns in the β-$Ca_3(PO_4)_2$-type structure with vacant *M*4 and *M*6 sites. The location of some $P1O_4$ tetrahedra is emphasized by the arrows. (b) Ferroelectric *R*3*c* phase. (a) Paraelectric $R\bar{3}m$ and (c) antiferroelectric $R\bar{3}c$ phases; 'idealized' orientations of $P1O_4$ tetrahedra in these phases are shown because in the average structures, $P1O_4$ tetrahedra are highly disordered.

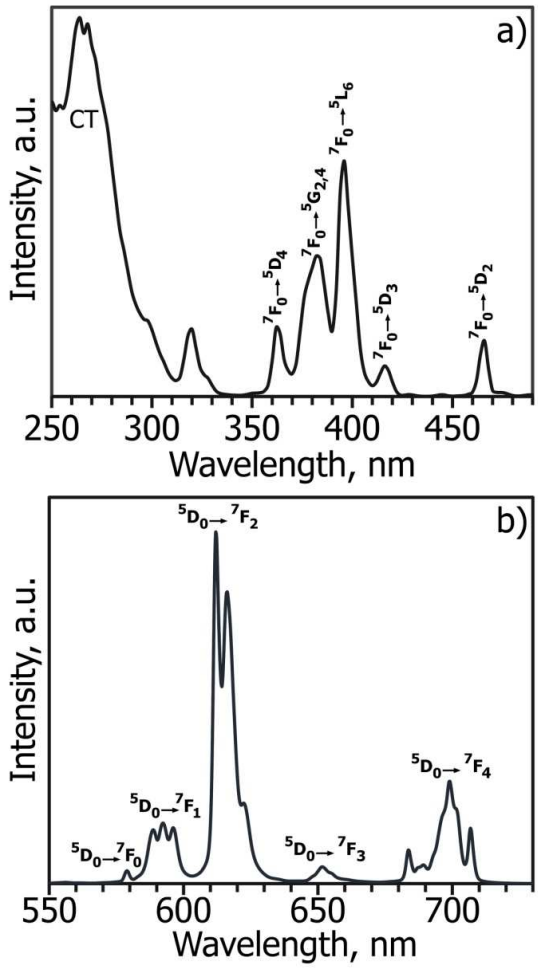

Fig. 10 (a) Room temperature photoluminescence excitation (λ_{em} = 615 nm) and (b) photoluminescence emission (λ_{ex} = 395 nm) spectra of $Ca_8MgEu(PO_4)_7$ (sample I). CT: charge transfer.

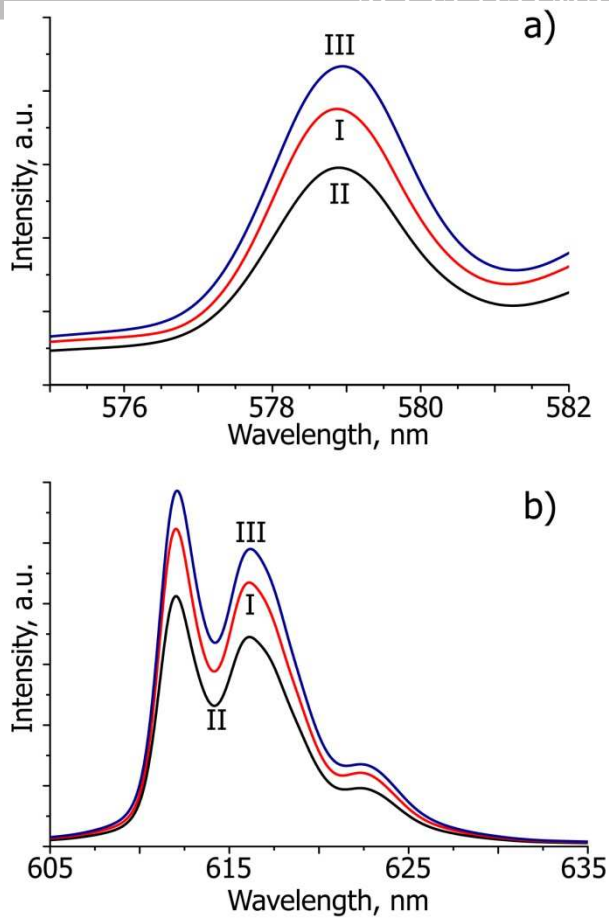

Fig. 11 Parts of room temperature photoluminescence emission spectra of $Ca_8MgEu(PO_4)_7$ (samples I, II, and III) for (a) $^5D_0 \rightarrow {}^7F_0$ and (b) $^5D_0 \rightarrow {}^7F_2$ transitions.

Crystal structures of $Ca_8MgR(PO_4)_7$ (R = rare-earth elements) luminescent materials were studied.

$Ca_8MgR(PO_4)_7$ crystallize in centrosymmetric space group R-3c in contrast to their parent compound.

Distribution of rare-earth elements among structural sites was established.

Antiferroelectric properties were detected in all samples.